*Available online www.jsaer.com*

***Journal of Scientific and Engineering Research*, 2017, 4(4):208-220**


**Research Article**

**ISSN: 2394-2630**
**CODEN(USA): JSERBR**

# Biaxial Mechanical Properties Simulation of Fiber-Metal Laminates

**Chengdong Li[1]*, Xiao Du[1], Jing He[2], Fengxing Ge[1]**

[1]Qinghai Normal University, Xining Qinghai, China 810008
[2]California State University Stanislaus, Turlock, CA, USA 95382

**Abstract** Fiber-metal laminates (FMLs) are materials designed for the aircraft industry applications, such as cargo door, upper fuselage and lower wing panels. They are composed of ductile aluminum layers with high strength fiber reinforced polymer layers. The three main types of FMLs investigated so far are based on aramid, glass and carbon fibers with aluminum alloys. FMLs with different metallic materials and polymer matrices are also introduced. Several important mechanical properties and test methods are discussed. It has been established that the off-axis angles of fibers affect the tensile properties significantly. As a result, multilayers with combinations of different fiber directions and fiber types have been used to face the complicated stress distributions in applications. So far, however, only uniaxial tests have been used to characterize the mechanical properties such as tensile and flexural strengths, which cannot reflect the real loading situation of the FML applications. So, biaxial tensile tests are suggested to characterize the overall tensile and flexural behavior when different off-axis angle combinations are present. To provide a theoretical basis for the multiaxial tests, a general multiaxial stress-strain analytical model based on classical laminate theory is proposed to guide experimental methods and compare the test results. This model can apply to various configurations of laminates, including multiple fiber off axis angles and both the elastic and plastic regions of stress-strain curves.

**Keywords** Fiber-Metal Laminates, strength, Biaxial

## 1. Introduction

Composite materials have been a research focus in various areas for decades [1-4]. The basic motivation is the possibility to take advantage of differing beneficial properties of the constituent materials [5-8]. The constituent materials have been employed with polymers [9], ceramics [10], nanomaterials [11-12], construction materials [13]. A unique combination among these was developed as stacking layers of fiber-reinforced polymers (FRPs) and metals, which are named as fiber-metal laminates (FMLs). The resulting composites have advantages of good corrosion resistance, fatigue resistance, impact resistance, flame resistance, static properties, and light weight [14-17]. Nowadays, the major applications of FML materials are for aircraft industries, such as the upper fuselage panels are made with GLARE.

One of the most important features of FML materials is that they take the advantage of fibers' ability to form a bridge in the fiber/polymer layer even when cracks happen in the metal layers. When failures happen in the metal layers, the FML still does not completely fail and the stress is redistributed in the composites layer. In this way, the fibers keep the cracks from further growing [18].

### 1.1. Three main types of FMLs

The three most common FMLs developed so far are Aramid Fiber Reinforced Aluminum Laminate (ARALL), Carbon Fiber Reinforced Aluminum Laminate (CARALL), and Glass Fiber Reinforced Aluminum Laminate (GLARE) [18]. ARALL was first made in 1978 by researchers at the National Laboratory and at the Delft University of Technology in the Netherlands in order to pursue an improved fatigue resistance performance of

aluminum composites, because aramid fibers have excellent specific strength, toughness, impact resistance and modulus [18, 19]. Until now, four different types of ARALL have been manufactured: ARALL 1-4 as Table 1 shows.

**Table 1**: The main features of the 4 grades of ARALL [18]

| | Metal type | Metal thickness (mm) | Fiber layer | Fiber direction (°) | Characteristics |
|---|---|---|---|---|---|
| ARALL 1 | 7075-T6 | 0.3 | 0.22 | 0/0 | Fatigue strength |
| ARALL 2 | 2024-T3 | 0.3 | 0.22 | 0/0 | Fatigue formability |
| ARALL 3 | 7475-T76 | 0.3 | 0.22 | 0/0 | Fatigue strength, exfoliation |
| ARALL 4 | 2024-T8 | 0.3 | 0.22 | 0/0 | Fatigue elevated temperature |

ARALL has been applied for the lower wing skin panels of the former Fokker 27 [18] the cargo door of American C-17 [20]. These are the only major applications for ARALL materials.

CARALL laminates contain carbon fiber reinforced prepregs instead of aramid fiber reinforced prepregs. CARALL is a strain rate sensitive material [21]. The tensile strength and failure strain increase significantly with increasing strain rate. According to one report [16], The CARALL has higher compressive strength values than GLARE.

GLARE is a stack composed of thin sheets of aluminum (AA2024-T3) bonded with glass fiber-reinforced adhesive layers, which are lay-ups of prepreg sheets made of high-strength unidirectional S2-glass fibers embedded in an epoxy matrix [22]. Generally, GLARE laminate was an on-going research focus after ARALL, emerging in 1987. GLARE has a better adhesive property between the glass fibers and the matrix compared with that of CARALL [18]. Unlike ARALL, GLARE is now widely applied in the aircraft industry, because of better mechanical properties such as the damage tolerance properties [23]. GLARE laminates are commercialized into six different standard grades as Table 2 shows.

**Table 2**: The major features of the six grades of GLARE [18]

| Grade | Sub | Metal type | Metal thickness (mm) | Fiber layer (mm) | Pregreg orientation in each fiber layer (°) | Characteristics |
|---|---|---|---|---|---|---|
| GLARE 1 | - | 7475-T761 | 0.3-0.4 | 0.266 | 0/0 | Fatigue, strength, yield stress |
| GLARE 2 | GLARE 2A | 2024-T3 | 0.2-0.5 | 0.266 | 0/0 | Fatigue, strength |
| | GLARE 2B | 2024-T3 | 0.2-0.5 | 0.266 | 90/90 | Fatigue, strength |
| GLARE 3 | - | 2024-T3 | 0.2-0.5 | 0.266 | 0/90 | Fatigue, impact |
| GLARE 4 | GLARE 4A | 2024-T3 | 0.2-0.5 | 0.266 | 0/90/0 | Fatigue, strength, in 0° direction |
| | GLARE 4B | 2024-T3 | 0.2-0.5 | 0.266 | 90/0/90 | Fatigue, strength, in 90° direction |
| GLARE 5 | - | 2024-T3 | 0.2-0.5 | 0.266 | 0/90/90/0 | Impact, shear, off-axis properties |
| GLARE 6 | GLARE 6A | 2024-T3 | 0.2-0.5 | 0.266 | 45/-45 | Shear, off-axis properties |
| | GLARE 6B | 2024-T3 | 0.2-0.5 | 0.266 | -45/45 | Shear, off-axis properties |

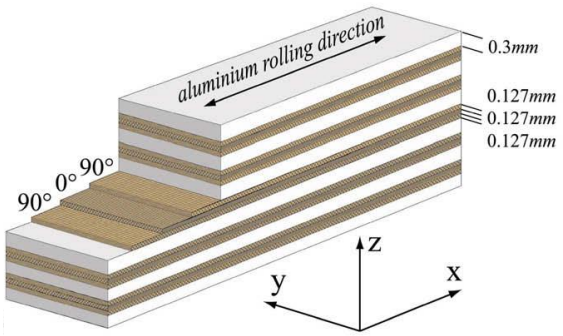


*Figure 1: Schematic description of Glare 4B-6/5-0.3*

Glare grade 4B-6/5-0.3, as Fig. 1 shows, consists of six aluminum layers with a nominal thickness of 0.3 mm. Five glass fiber reinforced polymer (GFRP) layers are between them. Each GFRP layer is stacked with three prepreg plies, with a nominal thickness of 0.127 mm, oriented in [90°, 0°, 90°] relative to the rolling direction of the aluminum [23]. GLARE laminates were chosen as the fuselage materials in the Airbus 380 and lower wing panels of the Fokker 27 [24] for their excellent fatigue properties.

Among the three different fibers, aramid fibers provide good specific strength and modulus, high impact resistance and toughness, while the low compressive strength is a disadvantage. In this point of view, CARALLs are developed to improve compressive strength relative to ARALLs, while it is noteworthy that CARALLs have relatively low strain to failure and impact resistance [18]. Other than compressive strength, the high stiffness of carbon fibers can provide efficient crack bridging and hence low crack growth rate [16]. The combination of high stiffness, strength and good impact properties make CARALL an advantage for space applications [16]. GLAREs are now the most widely used type among the three introduced above [25] because their high tensile strength and the low absorption of moisture compared with ARALLs [20] as well as good damage tolerance properties [25] and low cost. Compared with ARALL, GLARE has good fatigue properties and compressive loading as well as good impact and damage tolerance characteristics [25].

### 1.2. FML with different metals

Various types of aluminum alloys are chosen for FMLs because of their good properties such as high strength, low cost and low weight. For example, some properties of 2024-0 aluminum alloy are [26]: density of 2780 kg/m$^3$, melting point of 550 °C, tensile strength of 185 MPa, Young's modulus of 73.1 GPa and a strain to failure between 20% and 22%. Commercially available GLARE and ARALL based on aluminum offer some promising properties over traditional composites and monolithic metals, but the difficulty for them occurs at an elevated temperature, over 350 °C, due to the relatively low operating temperature of aluminum and epoxies, which is an obvious shortcoming. To solve this problem, an alternative metallic layer needs to be found for FML materials. Hundley et al. [27] did an investigation on the high temperature carbon fiber polyimide composites titanium FML. This class of FML is sometimes referred to as titanium-graphite, or TiGr, which is reported that not only have a high operating temperature, but also a higher stiffness and strength than GLARE and ARALL. One other choice for the metal layer is magnesium alloy as magnesium FMLs show features such as light weight, excellent corrosion resistance and electromagnetic shielding potential [28].

### 1.3. FML with different polymer matrices

The fiber/polymer composite layer plays an important role in determining the final mechanical properties of the whole FML. The first generation of FMLs was manufactured with thermosetting matrices for the composite layer, typically epoxy resins [18]. Since thermosetting-based FMLs suffer a number of disadvantages such as long processing cycles and low interlaminar fracture toughness properties [28], some other types of materials were chosen for the matrix, such as poly-ether-ether-ketone (PEEK) [29], self-reinforced polypropylene (SRPP) [26]. These are called thermoplastic materials, which have advantages including short processing times, ease of forming and repair [28].

As discussed above, with the choices and combinations of different fibers, polymer matrices and metals different types of FMLs can be made. There is no particular design which can perfectly satisfy all needs and provide superior properties than any other FMLs. It is mentioned above that Chang et al. [30] added a boron fiber-epoxy layer into the GLARE FMLs to increase the Young's modulus. The mixtures of different fibers with different off axis angles might be the simplest solution to create FML laminates with multiple advantages such as high strength, toughness, Young's modulus and impact resistance under complicated stress loadings. Recently, there are some work (discussed in later sections) focusing on the relationship between tensile properties and off axis angles of fiber directions, which provide some insights for further FML design. However, all these unidirectional tests are far from the loading configurations of FML applications, which carry much more complicated stress distributions. For example, the lower wings of aircrafts bear different stresses under the conditions of stable, moving upward and downward. Surprisingly so far, no multiaxial tests have been brought up to examine the FML materials when they are truly in need. In this paper, multiaxial tensile and flexural stress tests are proposed in Section 4 to measure the mechanical properties under multiaxial stress distributions. A universal analytical model based on classical laminate theory taking account of the elastic-plastic transformation of metallic layer is established in Section 3 to examine and compare experimental results.

### 1.4. FML preparation

Sinmazçelik et al. [18] give five activities in FML production, which are not discussed in detail in this paper: (1) Tools and raw materials preparation. (2) Materials deposition. (3) Cure preparation. (4) Cure. (5) Post stretching.

Autoclave processing is the most commonly used technique to produce FML laminates [31]. Some other researchers used a hand layup method to build the stacking [32]. In order for a better bonding between different layers, both mechanical and chemical surface treatment methods are applied to metals [18]. To further acquire an adhesive bonding between composites/metal interface, the curing temperature is normally much higher than room temperature (120 °C for GLARE [18]). When the FML materials are cooled down to room temperature, there would be a tensile stress in metal ply and compressive stress in fiber prepreg, which results in a residual stress in the laminates. Post-stretching is used to strain the metal layers into their plastic region, while the fiber layer remains elastic in the stress-strain curve [25]. It is noteworthy that when the residual stresses are present, the laminate stress distribution can also be analyzed with the analytical model proposed later.

## 2. Mechanical properties

Some important mechanical properties and test methods of FML materials are discussed in this section, including impact, tension, compression, shear, interfacial and flexural behavior.

### 2.1. Impact

Impact behavior is very important to FML materials, because a variety of objects can cause an impact on aircraft structures, such as bird strikes, hail and collision between cargo and the structure [33]. The failure mechanisms in impact behavior for metals and composites are quite different, especially for low-velocity impact behavior [34]. The damage on metals is visible while that for composites might be hidden [35]. This invisible damage can result in significant loss in materials strength [34], which makes it necessary to investigate the low impact behavior of FML materials. Since FML materials are aimed for the aircraft industry, the high velocity impact behavior is very important for FML materials. The high velocity impact behavior is defined when the sample is hit by a light-weight object which is travelling at a high speed [28]. The basic method to conduct a high velocity impact test is to use a gas gun to accelerate a projectile onto the specimen. The projectiles normally have velocities ranging from 25 to 100 m/s [18].

### 2.2. Tension

As a common mechanical test, tensile test provides information about important properties such as maximum stress, Young's modulus and strain to failure. The tensile strength test specimens are normally dog bone shape [21] or straight-sided shape [28]. The standards used for tensile testing include ASTM D3039 [32] and JIS

K7073 [16]. The tensile tests are performed at various crosshead speeds, from 0.1 mm/min to 5 mm/min [36]. In some studies, the test is carried out at a constant strain rate of 0.04 $min^{-1}$ [26]. A strain rate effect for tensile tests has been investigated [21].

2.3. Compression

The compressive strength for unidirectional composites is basically dominated by the buckling modes of the fibers [37]. Fig. 2 describes how laminates break during a compressive loading.

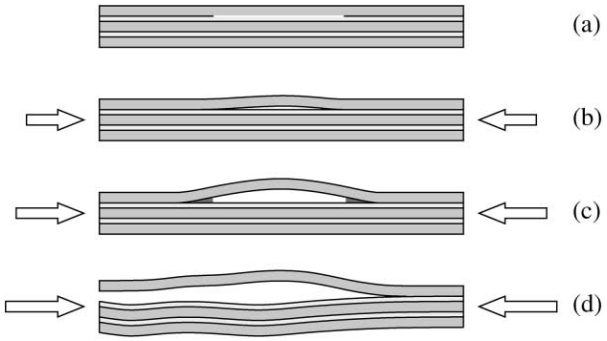


*Figure 2: Schematic representation of the delamination and buckling failure steps*

2.4. Shear, interfacial and flexural behavior

The flexural strength of FML materials is related to the interlaminar shear strength. So, these three mechanical properties are reviewed in this section.

The bending tests are all used for the FML tests, to provide information on interlaminar shear strength (ILSS). For example, the ILSS measured with five-point bending is determined as [38]:

$$\mathrm{ILSS} = \frac{33P_{max}}{64Wt}$$

In which $P_{max}$ is the failure load, W the width and t the thickness of the specimens.

Another method for investigating the interlaminar shear properties is the double notch shear test (DNS) test at room temperature according to ASTM D3846 [22]. When a compressive stress is applied to the specimen, the notched layers will have free space to move. Then, the only force that resists the final failure of the whole FML is the interlaminar shear force. Rather than bending tests, this method provides direct information about the interlamiar shear properties. Some other tests includes single cantilever beam (SCB), short beam shear test [18] and bonded window frame method [39]. All these developed testing methods, however, are uniaxial. For example, bending tests can only examine the longitudinal properties, which are not enough to simulate the flexural loadings on wing panels of aircrafts.

**3. Analytical Model**

One of the most important quasi-static properties of FML materials is the strain-stress relationship. Moussavi-Torshizi et al. [32] proposed a unixial stress-strain relationship which takes into account the elastic-plastic behavior of the aluminum sheets. Good agreement was shown between experimental results and the theoretical curves. The strengths for the pure elastic part and elastic-plastic part are given by the following two equations [32]:

$$\text{Elastic region: } \sigma_{FML} = \frac{E_{AL}\,t_{AL} + E_{FRP}\,t_{FRP}}{t_{FML}} \cdot \varepsilon_{FML}$$

$$\text{Plastic region: } \sigma_{FML} = (\sigma_y)_{AL}\,\frac{t_{AL}}{t_{FML}}\left(1 - \frac{E_{pl}}{E_{el}}\right)_{AL} + \frac{(E_{pl})_{AL}\,t_{AL} + E_{FRP}\,t_{FRP}}{t_{FML}} \cdot \varepsilon_{FML}$$

where $E_{AL}$ is the Young's modulus of Al, $t_{AL}$ the thickness of Al layer, $E_{FRP}$ the Young's modulus of fiber reinforced polymer (FRP) layer, $t_{FRP}$ the thickness of FRP layer, $t_{FML}$ the total thickness of FML, $\varepsilon_{FML}$ the strain

of laminate, $(\sigma_y)_{AL}$ the yield stress of Al, $E_{pl}$ the modulus of the plastic region, $E_{el}$ the modulus of the elastic region, $(E_{pl})_{AL}$ the modulus of Al at the plastic region.

This model was only established for unidirectional tensile tests, and hence the big limitation is that it can only solve the one-dimensional problems, which make it unrealistic for the FML applications. For multidirectional stress loading, a modified approach based on classical laminate theory is introduced here.

Stress-strain relationship of normal 3-demensional system can be written as follow:

$$\begin{pmatrix}\sigma_{xx}\\ \sigma_{yy}\\ \sigma_{zz}\\ \tau_{yz}\\ \tau_{xz}\\ \tau_{xy}\end{pmatrix}=\begin{pmatrix}C_{11} & C_{12} & C_{13} & C_{14} & C_{15} & C_{16}\\ C_{21} & C_{22} & C_{23} & C_{24} & C_{25} & C_{26}\\ C_{31} & C_{32} & C_{33} & C_{34} & C_{35} & C_{36}\\ C_{41} & C_{42} & C_{43} & C_{44} & C_{45} & C_{46}\\ C_{51} & C_{52} & C_{53} & C_{54} & C_{55} & C_{56}\\ C_{61} & C_{62} & C_{63} & C_{64} & C_{65} & C_{66}\end{pmatrix}\begin{pmatrix}\varepsilon_{xx}\\ \varepsilon_{yy}\\ \varepsilon_{zz}\\ 2\varepsilon_{yz}\\ 2\varepsilon_{xz}\\ 2\varepsilon_{xy}\end{pmatrix}$$

For laminate (plane stress) system, all stress components associated with Z-direction are zero values, and hence the equation can be rewritten as:

$$\begin{pmatrix}\sigma_1\\ \sigma_2\\ \sigma_6\end{pmatrix}=\begin{pmatrix}\sigma_{xx}\\ \sigma_{yy}\\ \sigma_{xy}\end{pmatrix}=\begin{pmatrix}Q_{11} & Q_{12} & Q_{16}\\ Q_{12} & Q_{22} & Q_{26}\\ Q_{16} & Q_{26} & Q_{66}\end{pmatrix}\begin{pmatrix}\varepsilon_1\\ \varepsilon_2\\ \varepsilon_6\end{pmatrix}$$

in which $(Q_{ij})$ is the reduced stiffness constant matrix [40]. Especially when the materials direction (the direction along the fiber for unidirectional FMLs) is orthotropic, $Q_{16}=Q_{26}=0$.

All the stiffness components can be expressed as functions of engineering constants in materials directions:

$$Q_{11}=\frac{E_L}{1-\nu_{LT}^2\frac{E_T}{E_L}}$$

$$Q_{22}=\frac{E_T}{E_L}Q_{11}$$

$$Q_{12}=\nu_{LT}Q_{22}$$

$$Q_{66}=G_{LT}$$

which are the basics for multiaxial stress analytical modeling [40]. In the functions, $E_L$ and $E_T$ are longitudinal and transverse Young's modulus, $\nu_{LT}$ the poisson's ratio and $G_{LT}$ the shear modulus. To acquire engineering constants for the $(Q_{ij})$ matrix, the mixtures laws are applied, which were used in the literatures [26].

$$E_L=E_fV_f+E_m(1-V_f)$$

$$E_T=\frac{E_m}{1+\left(\frac{E_m}{E_f}-1\right)V_f}$$

$$\frac{1}{G_{LT}}=\frac{V_f}{G_f}+\frac{1-V_f}{G_m}$$

$$\nu_{LT}=\nu_fV_f+\nu_m(1-V_f)$$

where, $E_f$, $V_f$, $G_f$ and $\nu_f$ are the Young's modulus, volume fraction, shear modulus and poisson's ratio for fibers, $E_m$, $G_m$ and $\nu_m$ the properties of polymer matrix. It is noteworthy that for isotropic materials, only two of the three properties E, G, ν are independent, in which case the following relationship can be applied to acquire the third property with two of them:

$$E=2G(1+\nu)$$

When there is an off-axis present, the matrix rotation can apply to transform the $(Q_{ij})$ matrix. The results are summarized as follow [40]:

$$Q_{11}^{'} = Q_{11}\cos^4\theta + Q_{22}\sin^4\theta + 2(Q_{12} + 2Q_{66})\cos^2\theta\sin^2\theta$$

$$Q_{12}^{'} = Q_{12}(\cos^4\theta + \sin^4\theta) + (Q_{11} + Q_{22} - 4Q_{66})\cos^2\theta\sin^2\theta$$

$$Q_{16}^{'} = (Q_{11} - Q_{12} - 2Q_{66})\cos^3\theta\sin\theta + (Q_{12} - Q_{22} + 2Q_{66})\sin^3\theta\cos\theta$$

$$Q_{22}^{'} = Q_{22}\cos^4\theta + Q_{11}\sin^4\theta + 2(Q_{12} + 2Q_{66})\cos^2\theta\sin^2\theta$$

$$Q_{26}^{'} = (Q_{11} - Q_{12} - 2Q_{66})\sin^3\theta\cos\theta + (Q_{12} - Q_{22} + 2Q_{66})\cos^3\theta\sin\theta$$

$$Q_{66}^{'} = Q_{66}(\cos^4\theta + \sin^4\theta) + (Q_{11} + Q_{22} - 2Q_{66} - 2Q_{12})\cos^2\theta\sin^2\theta$$

For now, the theoretical stress-strain curves can be plotted with ($Q_{ij}$) matrix regardless of layer stacking, fiber direction or in plane loading conditions. Due to the elastic-plastic transformation of the metallic layer, the curve is distinctively two-part. So in this model, Young's modulus of metallic layer is $E_{el}$ before yield and $E_{pl}$ after yield for ($Q_{ij}$) calculations.

## 4. Results

### 4.1. Orientation of fibers

To bring up the multiaxial tests and verify the feasibility of the stress-strain analytical model, FML materials with different fiber directions (orientations) are introduced here. Fiber orientation is a crucial factor to determine the final mechanical properties, such as tensile strength. Moussavi-Torshizi et al. [32] showed that a large off-axis angle significantly decreases the tensile strength of glass fiber and Kevlar (one type of aramid) fiber reinforced aluminum alloy, and that the Kevlar fiber orientation is the most important factor. In their work, the stack sequence is aluminum (AL) – glass/epoxy (GE) – Kevlar/epoxy (KE) – GE – AL. Nine groups of FMLs were made with different fiber orientations in the middle three layers, as Table 3 shows:

**Table 3**: The nine groups of specimens with different fiber orientations [32]

| Specimen code | Glass fiber orientation/$\theta_1$ (°) | Aramid fiber orientation/$\theta_2$ (°) |
|---|---|---|
| A | 0 | 0 |
| B | 0 | 45 |
| C | 0 | 90 |
| D | 45 | 0 |
| E | 45 | 45 |
| F | 45 | 90 |
| G | 90 | 45 |
| H | 90 | 90 |

With the tensile strength tests, it was found that the Young's modulus, yield stress and ultimate tensile stress all decrease with an increasing off-axis angle [32]. It is clear that, when a large off-axis angle is present, the fibers are not efficient in resisting the tensile force and bridging the crack. In real applications, the loading on the FML materials is normally multi-directional. For this reason, multi-axis tests can be helpful in assessing complicated loading mechanical properties. These tests suggested below are quasi-static and aimed for tensile, flexural behavior.

### 4.2. Biaxial Tensile Tests

#### 4.2.1. Square specimen

The test specimens will be stacked as those used in literature [32]: AL-GE-KE-GE-AL. The tensile test is performed by Instron 8502 (30 tons) apparatus.

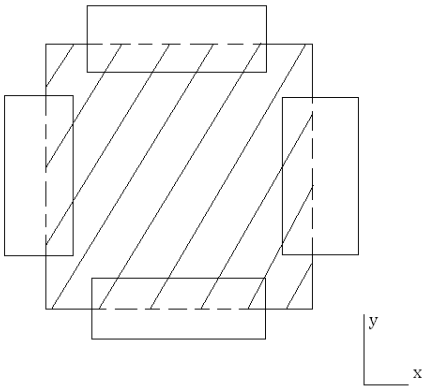


*Figure 3: Scheme of the biaxial tensile strength test on a square specimen*

As Fig. 3 shows, the square specimens are prepared in the dimensions of 225 mm × 225 mm × 3 mm. The clamp width is 125 mm and depth overlap with the specimen 20 mm. For the symmetry, it is unnecessary to test all the nine groups, but five of them, as shown in Table 4.

**Table 4**: The five groups of specimens with different fiber orientations

| Specimen code | Glass fiber orientation/$\theta_1$ (°) | Kevlar fiber orientation/$\theta_2$ (°) |
|---|---|---|
| A | 0 | 0 |
| B | 0 | 45 |
| C | 0 | 90 |
| D | 45 | 0 |
| E | 45 | 45 |

The loading rates for both directions are set as 0.2 mm/min.

The multiaxial stress-strain analytical modeling described in Section 3 can provide a theoretical basis for the test. With the same volume fraction 57% as in literature [32] and properties given below in Table 5:

**Table 5**: Properties of each components of the FML

| | aluminum AA 5086 | Kevlar fiber | Glass fiber | Epoxy |
|---|---|---|---|---|
| $E_{el}$ (GPa) | 46.5 | 120 | 73 | 2 |
| $E_{pl}$ (GPa) | 0.77 | - | - | - |
| ν | 0.33 [41] | 0.217 | 0.221 | 0.3 [40] |
| G (GPa) | 34.701 | 49.3 [40] | 29.9 [40] | 49.3 |

All other data are from [32] or calculations.

Now with these data and mixtures law, all composites properties $E_L$, $E_T$, $\nu_{LT}$, $G_{LT}$ can be determined. The second step is to create the (Qij) matrix with the composites properties. All calculated results at the off axis angle of 0° are show in Table 3:

**Table 6**: Parameters for stress-strain simulation at the 0° off axis

| | Aluminum alloy | Glass/epoxy | Kevlar/epoxy |
|---|---|---|---|
| $E_L$ (GPa) | 46.5 | 42.47 | 69.26 |
| $E_T$ (GPa) | 46.5 | 4.488 | 4.551 |
| $\nu_{LT}$ | 0.33 | 0.255 | 0.253 |
| $G_{LT}$ (GPa) | 34.701 | 3.125 | 3.205 |
| $Q_{11}$ (GPa) | 52.183 | 42.764 | 69.553 |
| $Q_{22}$ (GPa) | 52.183 | 4.519 | 4.57 |
| $Q_{12}$ (GPa) | 17.22 | 1.152 | 1.156 |
| $Q_{66}$ (GPa) | 34.701 | 3.125 | 3.205 |

With the transformation of rotation introduced in Section 3.2, the ($Q'_{ij}$) matrix at the off-axis angle of 90° and 45° can be attained as Table 7 and 8 show:

**Table 7**:. Parameters for stress-strain simulation at the 45° off axis

| | **Glass/epoxy** | **Kevlar/epoxy** |
|---|---|---|
| $Q_{11}$(45°) (GPa) | 15.522 | 22.314 |
| $Q_{22}$(45°) (GPa) | 15.522 | 22.314 |
| $Q_{12}$(45°) (GPa) | 9.272 | 15.904 |
| $Q_{66}$(45°) (GPa) | 11.245 | 17.953 |
| $Q_{16}$(45°) (GPa) | 9.561 | 16.246 |
| $Q_{26}$(45°) (GPa) | 9.561 | 16.246 |

**Table 8**: Parameters for stress-strain simulation at the 90° off axis

| | **Glass/epoxy** | **Kevlar/epoxy** |
|---|---|---|
| $Q_{11}$(90°) (GPa) | 4.519 | 4.57 |
| $Q_{22}$(90°) (GPa) | 42.764 | 69.553 |
| $Q_{12}$(90°) (GPa) | 1.152 | 1.156 |
| $Q_{66}$(90°) (GPa) | 3.125 | 3.205 |
| $Q_{16}$(90°) (GPa) | 0 | 0 |
| $Q_{26}$(90°) (GPa) | 0 | 0 |

It is noteworthy that when the off-axis is 45° (actually for all angles other than 0° and 90°), the two components $Q_{16}$(45°) and $Q_{26}$(45°) are not zero values anymore, which result in a none-zero shear stress term $\sigma_{xy}$. In actual tensile testing, this term is regarded as trivial in affecting the normal stress measured. So it is not taken into account in determining the normal stress-strain relationship.

The yield point is determined with the von Mises yield criterion:

$$(\sigma_1 - \sigma_2)^2 + (\sigma_2 - \sigma_3)^2 + (\sigma_3 - \sigma_1)^2 = 2\sigma_y^2$$

For 2D problem, the yield surface is determined as:

$$\sigma_1^2 + \sigma_2^2 - \sigma_1\sigma_2 = \sigma_y^2$$

When the strain rates at x- and y- axis are the same, the yield criterion is simplified as:

$$\sigma_1 = \sigma_y$$

With a simple mixtures rule [26] of all laminate layers, the stress measured can be attained with following equation:

$$\sigma_{FML} = \frac{\mathbf{Q}_{AL}t_{AL} + \mathbf{Q}_{GE}t_{GE} + \mathbf{Q}_{KE}t_{KE}}{t_{FML}}\varepsilon$$

in which, $t_{AL}$, $t_{GE}$, $t_{KE}$ and $t_{FML}$ are the layer thickness of aluminum alloy, glass/epoxy, Kevlar/epoxy, and the total FML material, **Q** is the corresponding stiffness components for each layer.

After yield, all AL related parameters should be calculated with $E_{pl}$ rather than $E_{el}$, in this which case, the ($Q_{ij}$) components needed for calculations are listed in Table 7.

**Table 9**: Reduced stiffness components after metallic layer yield.

| | **AL after yield** |
|---|---|
| $Q_{11}$ (GPa) | 0.864 |
| $Q_{22}$ (GPa) | 0.864 |
| $Q_{12}$ (GPa) | 0.285 |

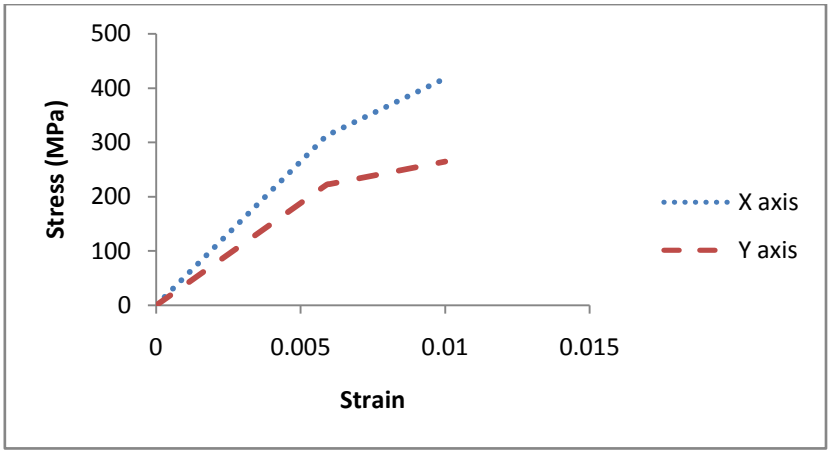


*Figure 4: The stress-strain relationships for specimen B (0°-45°-0°)*

Taking specimen B (0°-45°-0°) as an example, the stress-strain relationships are plotted in Fig. 4. According to von Mises criterion, the theoretical yield points for the two directions happen at the same time since the strain rates are set as the same.

4.2.2. Rectangular specimen

The test method above is basically an isotropic test: the shape of specimen is squared and the strain rates are the same. In order to observe specimen tensile behavior under anisotropic stress loadings, the tensions are performed on the rectangular specimen on x-y direction.

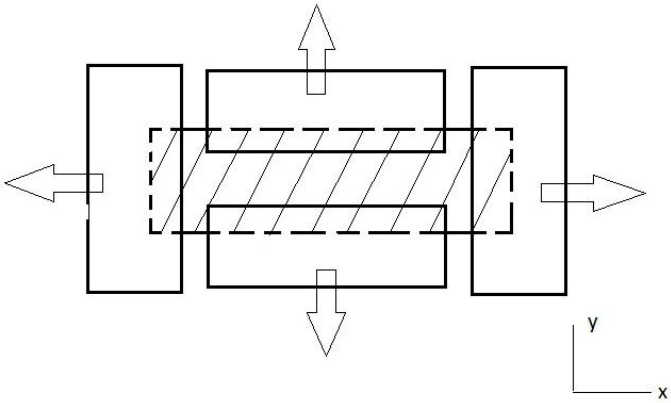


*Figure 5: Scheme of the biaxial tensile strength test on a rectangular specimen*

The straight-sided specimens are cut to the dimensions of 225 mm × 75 mm × 3 mm. The test set-up is as Fig. 5 shows. The two narrow ends are totally clamped, while the two wide sides are partly clamped. The test matrix is the same one as Table 4. The clamp width is 125 mm and overlap with the specimen 20 mm.

For this test set-up, it is designed that the tension in x-axis is the main loading while the one along y-axis is an interference loading. The loading rates can be set as 2 mm/min in x-axis while 0.02 mm/min in y-axis. The main purpose is to observe how the tensile properties would be affected with a slight interference in other directions. Also the multiaxial stress-strain modeling can be easily applied on this rectangular specimen testing.

4.2.3. Two-step tensile tests

It is expected to face the difficulty to build the test set-ups for a multidirectional tensile test. An alternative two-step measurement of the tensile strength in x and y axis is proposed here. The specimens with dimensions of 225 mm × 225 mm × 3 mm are prepared. In the first step, the specimen is tested in the x axis and the second step the specimen is loaded in the y axis. However, a major difference with all tensile tests above is that the first-step measurement is not stopped when a complete failure is obtained. This is because when a final crack happens, the

measurement in the y direction cannot collect useful data for that the specimen is now two fragments rather than an intact piece. The stop for the first step is set at an offset point at 0.5% of the strain as Fig. 6 shows.

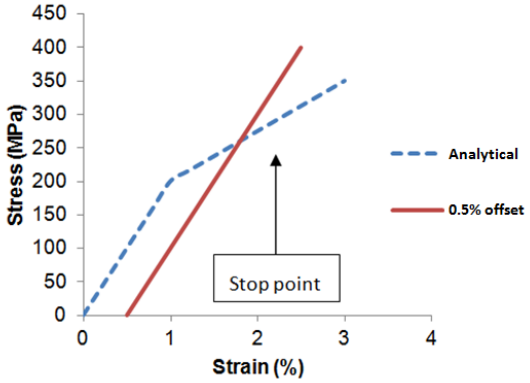


*Figure 6: The method of find the point to stop the first-step tensile test*

The selection of the offset value as 0.5% is based on published experimental results [32]. When the offset value is chosen as 0.5%, the stop point is still far from the final failure for all nine samples. On the other hand, the stop is not too close to the yield point. This would guarantee that, when the first-step tension is finished, all specimens are at the same mechanical state. It is noteworthy that: (1) The difficulty to perform this experiment is that, during the test, the strain-stress curve needs to be seen immediately on a screen, so that the stop point can be determined as soon as the first elastic part of the curve is clearly observed. (2) A shortcoming is that this method cannot provide the ultimate strength during the first step. (3) Because there is a sequence to perform the two steps of tensile tests, the x-axis first and y-axis second, there is no symmetry. All of the nine groups of specimens instead of five need to be done to collect enough data at different off-axis angles. Obviously the second step of the tensile strength test is performed when the yield point has been reached in the x axis. So, it would be interesting to compare the strain-stress curve in the y axis with a normal unidirectional tensile test to see if the yield in the x direction has a major effect on the tensile behavior at the y direction. It is expected the influence is very different at different off-axis angles. While the multiaxial model can still be applied on this two-step test, the second step can be simulated with $E_{pl}$ related functions.

## 5. Conclusion

The fiber-metal laminate (FML) materials are comprehensively reviewed. There are three main types of FMLs with respect to the fiber choice: ARALL with aramid fibers, CARALL with carbon fibers and GLARE with glass fibers. Among these three types, the GLARE is the most commonly used one in the aircraft industries due to the excellent mechanical properties and low cost. Other FMLs with different metallic materials and polymer matrix are also introduced. Several important mechanical properties and the test methods are reviewed. It is established that the off-axis angles of fibers affect the tensile behavior significantly. As well developed as these mechanical tests, however, the uniaxial tensile tests are not close to simulate the real situation of the applications and enough to examine the materials properties under complicated stress distributions. So biaxial tensile tests are suggested to characterize how the different off-axis angles combinations affect the overall tensile and flexural behavior with a complicated stress distribution. The specimens suggested are a mixed FML material with glass fiber layers and Kevlar fiber layer. To provide a theoretical basis, a multiaxial stress-strain analytical model based on classical laminate theory is proposed to simulate and compare the experimental data. This model applies in various stress distributions, with different combinations of fiber off-axis angles and strain rates in different directions.

## References

[1]. J. Yang, C. Han, Mechanically Viscoelastic Properties of Cellulose Nanocrystals Skeleton Reinforced Hierarchical Composite Hydrogels, ACS Applied Materials & Interfaces, 8 (2016) 10.

[2]. E.T. Thostenson, T.-W. Chou, Aligned multi-walled carbon nanotube-reinforced composites: processing and mechanical characterization, Journal of Physics D: Applied Physics, 35 (2002) 4.
[3]. Y. Cao, P. Zavaterri, J. Youngblood, R. Moon, J. Weiss, The influence of cellulose nanocrystal additions on the performance of cement paste, Cement and Concrete Composites, 56 (2015) 11.
[4]. W. Cai, B. Wu, N. Wu, 2.4 GHz Class F Power Amplifier for Healthcare Application, International Journal of Computer Science and Information Technologies, 7 (2016) 5.
[5]. Y. Cao, P. Zavattieri, J. Youngblood, R. Moon, J. Weiss, The relationship between cellulose nanocrystal dispersion and strength, Construction and Building Materials, 119 (2016) 9.
[6]. W. Cai, L. Huang, N. Wu, Class E Power Amplifier for Wireless Medical Sensor Network, International Journal of Enhanced Research in Science, Technology & Engineering, 5 (2016) 6.
[7]. H.P.S.A. Khalil, A.H. Bhat, A.F.I. Yusra, Green composites from sustainable cellulose nanofibrils: A review, Carbohydrate Polymers, 87 (2012) 17.
[8]. W. Cai, L. Huang, W. Wen, 2.4GHZ Class AB Power Amplifier for Wireless Medical Sensor Network, International Journal of Enhanced Research in Science, Technology & Engineering, 5 (2016) 5.
[9]. Y. Yang, X. Ding, M.W. Urban, Chemical and physical aspects of self-healing materials, Progress in Polymer Science, 49-50 (2015) 26.
[10]. T. Kosmač, C. Oblak, P. Jevnikar, N. Funduk, L. Marion, The effect of surface grinding and sandblasting on flexural strength and reliability of Y-TZP zirconia ceramic, Dental Materials, 15 (1999) 8.
[11]. Y. Cao, N. Tian, D. Bahr, P.D. Zavattieri, J. Youngblood, R.J. Moon, J. Weiss, The influence of cellulose nanocrystals on the microstructure of cement paste, Cement and Concrete Composites, 76 (2016) 10.
[12]. Y. Cao, Nano-modification for high performance cement composites with cellulose nanocrystals and carbon nanotubes, PhD Dissertation, (2014).
[13]. K. Sobolev, Z. Lin, Y. Cao, H. Sun, I. Flores-Vivian, T. Rushing, T. Cummins, W.J. Weiss, The influence of mechanical activation by vibro-milling on the early-age hydration and strength development of cement, Cement and Concrete Composites, 71 (2016) 10.
[14]. G. Wu, J.-M. Yang, The mechanical behavior of GLARE laminates for aircraft structures, Journal of The Minerals, Metals & Materials Society, 57 (2005) 8.
[15]. S.L. Lemanski, G.N. Nurick, G.S. Langdon, M.S. Simmons, W.J. Cantwell, G.K. Schleyer, Understanding the behaviour of fibre metal laminates subjected to localised blast loading, Composite Structures, 76 (2006) 6.
[16]. E.C. Botelho, R.A. Silva, L.C. Pardini, M.C. Rezende, A review on the development and properties of continuous fiber/epoxy/aluminum hybrid composites for aircraft structures, Materials Research, 9 (2006) 10.
[17]. W. Cai, J. Gong, N. Wu, 2.4GHZ Class F Power Amplifier for Wireless Medical Sensor Network, Proceedings of the 2nd World Congress on New Technologies, (2016) 7.
[18]. T. Sinmazçelik, E. Avcu, M.Ö. Bora, O. Çoban, A review: Fibre metal laminates, background, bonding types and applied test methods, Materials & Design, 32 (2011) 15.
[19]. Y. Cao, J. Weiss, J. Youngblood, R. Moon, P. Zavattieri, Performance-enhanced cementitious materials by cellulose nanocrystal additions, Production and Applications of Cellulose Nanomaterials, (2013) 2.
[20]. P.V. Straznicky, J.F. Laliberté, C. Poon, A. Fahr, Applications of fiber-metal laminates, Polymer Composites, 21 (2000) 10.
[21]. Y. Xia, Y. Wang, Y. Zhou, S. Jeelani, Effect of strain rate on tensile behavior of carbon fiber reinforced aluminum laminates, Materials Letters, 61 (2007) 3.
[22]. S. Hinz, T. Omoori, M. Hojo, K. Schulte, Damage characterisation of fibre metal laminates under interlaminar shear load, Composites Part A: Applied Science and Manufacturing, 40 (2009) 7.
[23]. S.U. Khan, R.C. Alderliesten, R. Benedictus, Delamination in Fiber Metal Laminates (GLARE) during fatigue crack growth under variable amplitude loading, International Journal of Fatigue, 33 (2011) 12.

[24]. E.M. Castrodeza, F.L. Bastian, J.E.P. Ipiña, Fracture toughness of unidirectional fiber–metal laminates: crack orientation effect, Engineering Fracture Mechanics, 72 (2005) 12.
[25]. S.U. Khan, R.C. Alderliesten, R. Benedictus, Post-stretching induced stress redistribution in Fibre Metal Laminates for increased fatigue crack growth resistance, Composites Science and Technology, 69 (2009) 10.
[26]. J.G. Carrillo, W.J. Cantwell, Mechanical properties of a novel fiber–metal laminate based on a polypropylene composite, Mechanics of Materials, 41 (2009) 11.
[27]. J.M. Hundley, H.T. Hahn, J.-M. Yang, A.B. Facciano, Three-dimensional progressive failure analysis of bolted titanium-graphite fiber metal laminate joints, Journal of Composite Materials, 45 (2011) 19.
[28]. P. Cortés, W.J. Cantwell, The fracture properties of a fibre–metal laminate based on magnesium alloy, Composites Part B: Engineering, 37 (2006) 8.
[29]. P. Cortes, W.J. Cantwell, The Tensile and Fatigue Properties of Carbon Fiber-reinforced PEEK-Titanium Fiber-metal Laminates, Journal of Reinforced Plastics and Composites, 23 (2004) 9.
[30]. P.-Y. Chang, P.-C. Yeh, J.-M. Yang, Fatigue crack initiation in hybrid boron/glass/aluminum fiber metal laminates, Materials Science and Engineering: A, 496 (2008) 8.
[31]. A. Vlot, J.W. Gunnink, Fibre Metal Laminates: An Introduction, Springer Science & Business Media, (2011).
[32]. S.E. Moussavi-Torshizi, S. Dariushi, M. Sadighi, P. Safarpour, A study on tensile properties of a novel fiber/metal laminates, Materials Science and Engineering: A, 527 (2010) 6.
[33]. L.B. Vogelesang, A. Vlot, Development of fibre metal laminates for advanced aerospace structures, Journal of Materials Processing Technology, 103 (2000) 5.
[34]. M.O.W. Richardson, M.J. Wisheart, Review of low-velocity impact properties of composite materials, Composites Part A: Applied Science and Manufacturing, 27 (1996) 9.
[35]. N. Tsartsaris, M. Meo, F. Dolce, U. Polimeno, M. Guida, F. Marulo, Low-velocity impact behavior of fiber metal laminates, Journal of Composite Materials, 45 (2011) 12.
[36]. S.M.R. Khalili, R.K. Mittal, S.G. Kalibar, A study of the mechanical properties of steel/aluminium/GRP laminates, Materials Science and Engineering: A, 412 (2005) 4.
[37]. D. Hull, T.W. Clyne, An Introduction to Composite Materials, Cambridge University Press, (1996).
[38]. C.M. Cepeda-Jiménez, R.C. Alderliesten, O.A. Ruano, F. Carreño, Damage tolerance assessment by bend and shear tests of two multilayer composites: Glass fibre reinforced metal laminate and aluminium roll-bonded laminate, Composites Science and Technology, 69 (2009) 6.
[39]. L. Boni, A. Lanciotti, L. Lazzeri, Experimental Tests and Numerical Analyses of Fiber Metal Laminate Panels under Shear Load with Bonded Window Frame, Journal of Composite Materials, 43 (2009) 22.
[40]. J.-M. Berthelot, Composite Materials Mechanical Behavior and Structural Analysis, Springer, 1999.
[41]. http://en.wikipedia.org/wiki/Poisson%27s_ratio.